Spectroscopy and Photophysics of 1,4-Bis(phenylethynyl)benzene: Effects of Ring Torsion and Dark $\pi\sigma^*$ State

Takashige Fujiwara,*,† Marek Z. Zgierski,‡ and Edward C. Lim*,†,§

Department of Chemistry and The Center for Laser and Optical Spectroscopy, The University of Akron, Akron, Ohio 44325-3601, and Steacie Institute for Molecular Sciences, National Research Council of Canada, Ottawa, K1A 0R6 Canada

Received: November 20, 2007; Revised Manuscript Received: January 23, 2008

A combination of supersonic-jet laser spectroscopy and quantum chemistry calculation was applied to 1,4-bis(phenylethynyl)benzene, BPEB, to study the role of the dark $\pi\sigma^*$ state on electronic relaxation and the effect of ring torsion on electronic spectra. The result provides evidence for fluorescence break-off in supersonic jet at high $S_1(\pi\pi^*) \leftarrow S_0$ excitation energies, which can be attributed to the $\pi\pi^*-\pi\sigma^*$ intersection. The threshold energy for the fluorescence break-off is much larger in BPEB ($\sim$4000 cm^{-1}) than in diphenylacetylene ($\sim$500 cm^{-1}). The high-energy barrier in BPEB accounts for the very large fluorescence quantum yield of the compound (in solution) relative to diphenylacetylene. The comparison between the experimentally derived torsional barrier and frequency with those from the computation shows overall good agreement and demonstrates that the low-energy torsional motion involves the twisting of the end ring in BPEB. The torsional barrier is almost an order of magnitude greater in the $\pi\pi^*$ excited state than in the ground state. The finding that the twisting of the end ring in BPEB is relatively free in the ground state, but strongly hindered in the excited state, provides rationale for the well-known temperature dependence of the spectral shape of absorption and the lack of mirror symmetry relationship between the absorption and fluorescence at elevated temperatures.

Introduction

Photophysics and spectroscopy of oligo(phenylethynyl)benzenes have received considerable attention recently due to efficient electronic communication between adjacent chromophores that has application in the design and fabrication of electroluminescent, semiconductor, and nonlinear optical materials.[1,2] Interestingly, the two smallest and most extensively studied members of this family of compounds, namely diphenylacetylene (DPA) and 1,4-bis(phenylethynyl)benzene (BPEB, shown below), display very different fluorescent properties. Thus

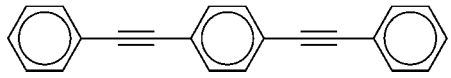

unlike DPA, which has very small fluorescence yield (Φ_F = 0.006)[3] and exhibit strong thermal quenching of fluorescence[4] in solution, BPEB is strongly fluorescent (Φ_F = 0.58)[3] and shows only weak dependence of its emission on temperature.

We have previously shown[5] that both the strong temperature dependence of fluorescence in solution and the abrupt break-off (loss) of fluorescence in jet-cooled DPA,[6] which occurs at excitation energy only slightly above the electronic origin of the fluorescent $\pi\pi^*$ state, could be rationalized by the crossing of the $\pi\pi^*$ state by a dark electronic state. The dark state was identified (by TDDFT and CASSCF calculations) as the $\pi\sigma^*$ state of bent geometry (with C≡C—C_{ph} angle of about 120°) that arises from the promotion of an electron from the phenyl π orbital to the σ^* orbital localized on the acetylene unit.[5] The occurrence of an activated state switch from the initially excited $\pi\pi^*$ state to the dark $\pi\sigma^*$ state is supported by the experimental observation of the strong picosecond transient at about 700 nm,[7,8] and the greatly reduced frequency ($\sim$1570 cm^{-1})[9] of the acetylene C≡C stretch, which are predicted[5] for the $\pi\sigma^*$ state. Consistent with the state switch, the decay time of the $\pi\pi^*$ picosecond transient at 500 nm was found to be identical to the risetime of the $\pi\sigma^*$ transient at 700 nm.[7]

In this paper, we extend the experimental and computational work, carried out for DPA, to BPEB. Because of the longer (more extended) π-conjugation in BPEB, which stabilizes the $\pi\pi^*$ state, some significant differences in the energy of the $\pi\pi^*$ state relative to the $\pi\sigma^*$ state may be expected between BPEB and DPA. The dramatically greater fluorescence yield of BPEB relative to DPA in fact suggests that the $^1\pi\pi^* \rightarrow {}^1\pi\sigma^*$ state switch, leading to quenching of fluorescence, may be much less efficient in BPEB as compared to DPA. We also address the strong temperature dependence of the spectral shape of $S_1 \leftarrow S_0$ absorption, which leads to the breakdown of the mirror symmetry relationship between the absorption and fluorescence at elevated temperatures.

Experimental and Theoretical Methods

1. Fluorescence Excitation Spectra. 1,4-Bis(phenylethynyl)benzene, BPEB, was used as received (Oakwood Products, 98%). The sample was heated to $\sim$180 °C by a film heater that surrounded a sample reservoir. Pulsed molecular jet (10 Hz) was formed by expanding a seeded BPEB in He at a pressure of up to 2 atm through a solenoid-driven valve (Parker; GV-9) with orifice of 0.8 mm. Fluorescence excitation (FE) measurements (resolution of $\sim$0.3 cm^{-1}) were performed with the frequency-doubled tuneable dye laser (Lambda Physik, Scan-Mate 2E) pumped by a Nd:YAG laser (Continuum, NY61-10)

* Corresponding authors. T.F.: e-mail, fujiwara@uakron.edu; fax: +1 (330) 972-6407. E.C.L.: e-mail, elim@uakron.edu.
† The University of Akron.
‡ Steacie Institute for Molecular Sciences.
§ The Holder of Goodyear Chair in Chemistry.

10.1021/jp711064g CCC: $40.75
Published on Web 05/06/2008

or a XeCl excimer laser (Lambda Physik, COMPex102). Several laser dyes were used to cover an entire spectral range (31000−38000 cm^{-1}). Fluorescence was collected at right angles to the jet and the laser by a lens that focused the emission onto a photomultipler tube, PMT (Hamamatsu; R955). Several cutoff filters were used to eliminate any laser light scattering. The signal from the PMT was preamplified and fed to a boxcar integrator (Stanford, SR250) and then transmitted *via* an interface module (Stanford; SR245) through a PC that collected and stored the data. The Laser wavelengths were calibrated using a Ne/Fe hollow cathode lamp (an accuracy of ±0.2 cm^{-1}).

Given that FE spectra of BPEB are prone to be saturated because of the presence of the low frequency vibrations, we kept input power as low as possible but employed an active attenuation technique to maintain a constant input fluence over tuning wavelengths of a dye laser output. In this technique a photoelastic modulator (Hinds, PEM-90) combined with a UV-grade Glan-Tayler polarizer (Karl Lambrecht) plays a key role. The modulator controlled by a PC variably rotates polarization of a lineally polarized laser light at any wave-retardation, and the polarizer filter reduces overall throughput. Monitoring an actual input fluence entering a vacuum chamber with a PMT (or a PD) as a feedback to an amount of changes of retardation enables us to actively lock (flatten out) an input fluence at a desired level over a wide-tuning range of a dye laser. It also helps quantitative comparisons on FE spectra recorded over several laser dyes.

2. Fluorescence Lifetime. The fluorescence time profile measurements employed a time-correlated single-photon counting (TCSPC) technique implemented by a picosecond laser system. The pulse-train from a dye laser (Coherent; 702−1D), synchronously pumped by a frequency doubling of a mode-locked 76 MHz Nd:YLF laser (Quantronix, 4217 ML), was cavity-dumped to typically <10 MHz. The laser pulse of ∼ 3 ps width was then focused into a BBO crystal to generate second harmonic radiation. The UV light crossed the jet at a distance of 2−4 mm downstream from a continuous-wave (CW) nozzle which has a metal pinhole of 100 μm operating at typical stagnation pressure of ∼ 3 atm with He carrier gas. The nozzle temperature with sample reservoir was automatically stabilized at ∼200 °C by means of a relay circuit. A high gas-flow from the CW nozzle was pumped with a 10" diffusion pump (Varian VHS-10; 6600 *l*/s) backed by a rotary pump (Edwards; E2M80) through a mechanical booster pump (Edwards; EH500A). The fluorescence was collected with a two-lens system and imaged a microchannel plate photomultiplier (MCP, Hamamatsu; R3809U-51), after passing though a cutoff filter or a high-throughput monochromator (Jarrel-Ash). The output of the MCP was fed to an onboard TCSPC module (Becker & Hickl, SPC-300) as a start pulse. Stop pulses were provided from a photodiode (EOT; ET2000), which monitored the residual of the fundamental pulses. The temporal response of the detection system was less than 30 ps (fwhm). The fluorescence temporal profiles were derived by deconvolution procedures with the instrumental response, using nonlinear least-squares fittings.

3. Computation. The ground and excited-state geometries were optimized with the HF and CIS methods, respectively, using correlation corrected cc-pVDZ basis set. Rotation of phenyl rings was investigated by optimizing with a fixed dihedral angle between the two rings and keeping two rings that did not rotate in the same plane. For S_0 calculated geometries, the vertical electronic energies were calculated with either the CIS or TD/B3LYP method. The Franck−Condon (FC) structure of the absorption/emission spectra was calculated by projecting the difference of optimized geometries of the two electronic states involved in the transition onto the normal coordinates of the final state. The displacement parameters for totally symmetric modes were then used to calculate FC factors for individual vibronic transitions. These individual transition were broadened with a Gaussian line-shape of a given half-width to produce the calculated vibronic structure of the electronic transition.

The barrier between the $\pi\pi^*$ and the bent $\pi\sigma^*$ state was found by partial CIS optimization of the initial (D_{2h} symmetry, linear molecule) $^1B_{1u}$ ($\pi\pi^*$) and the lowest 1A″ state under C_s symmetry when the C_{Ph}—C≡C angle on one acetylene unit deviates from 180°. This state becomes ultimately the lowest $\pi\sigma^*$ state at the C_{Ph}—C≡C angle near 125°. For such partially optimized CIS geometries of the 1A″ state (the $\pi\pi^*$ state is then of the 2A′ nature) the TD/BP86 vertical electronic energies were calculated at the TD/BP86 level of theory.

Results and Discussion

1. Fluorescence Excitation Spectrum Line Width, and Fluorescence Lifetime. Figure 1 displays the fluorescence excitation (FE) spectrum and excitation energy dependence of fluorescence lifetime and line width, for jet-cooled BPEB in the range of 31000−37800 cm^{-1}. Also shown, for comparison with the FE spectrum, is the vapor phase absorption spectrum of BPEB in the same spectral range. The origin band of BPEB at 31214 cm^{-1} is more than 4000 cm^{-1} red-shifted compared to that of DPA at 35248 cm^{-1}.

It is evident from the figure that the vibronic bands that are sharp and intense at low energies become broad and very weak at higher energies (>3500 cm^{-1}). More specifically, high-energy vibronic bands are significantly weaker in the FE spectrum as compared to the vapor phase absorption spectrum. Concomitantly, the line width of the high-energy bands is much broader than that of the low-energy bands (<2500 cm^{-1}) in the FE spectra. The greatly reduced fluorescence intensity and the significantly increased line width at high S_1 excess energies could be rationalized if the high-lying vibronic levels belong to another $\pi\pi^*$ state that rapidly decay nonradiatively through their interactions with the dense vibronic manifold of the $S_1(\pi\pi^*)$ state. This possibility is, however, very unlikely, as TDDFT calculations do not reveal the existence of any allowed $\pi \rightarrow \pi^*$ transition within 0.9 eV (∼7200 cm^{-1}) of the S_1 state. The calculated vertical excitation energies and oscillator strengths are given in Table 1. A much more likely explanation for the decrease in the emission intensity, and the increase in the spectral line width, at higher excitation energies is the nonadiabatic interaction of the $\pi\pi^*$ state with a dark electronic state that leads to a large decrease in the radiative decay rate of the initially excited $^1\pi\pi^*$ state.[10] The threshold energy for fluorescence break-off in supersonic jet is much greater for BPEB (∼4000 cm^{-1}) than in DPA (∼500 cm^{-1}).

The conclusion that the loss of fluorescence at higher excitation energy is due to a large decrease in the radiative decay rate (k_r) of the $S_1(\pi\pi^*)$ state, by its coupling to a dark electronic state, is supported by the measurement of fluorescence lifetime as a function of excitation energy (see Figure 1). Unlike the fluorescence intensity that drops off precipitously at higher S_1 excess energies, the fluorescence lifetime exhibits only a small monotonous decrease with increasing excess energy. Thus, the lifetime of 856 ps at the origin band (+0 cm^{-1}) decreases to 566 ps at the S_1 excess energy of 0 + 4871 cm^{-1}. Because the fluorescence quantum yield (Φ_F) is related to the fluorescence lifetime (τ_F) and k_r by $\Phi_F = k_r\tau_F$, the result demonstrates that

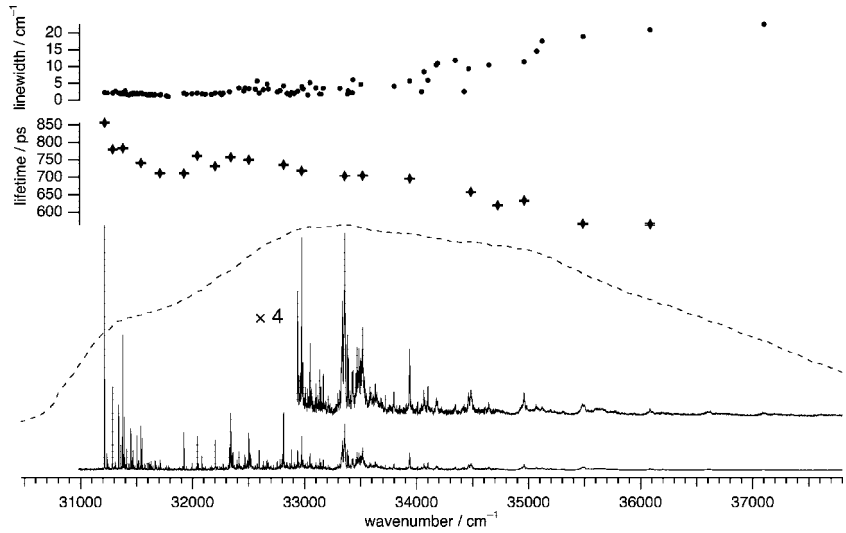

Figure 1. Florescence excitation spectra and excitation energy dependence of fluorescence lifetime (diamond) and spectral line width (dot) for jet-cooled 1,4-bis(phenylethynyl)benzene (BPEB) in the range 31000−37800 cm^{-1}. Also shown is a vapor phase absorption spectrum (dashed curve, from ref 12 with permission). To minimize spectral saturation, the FE spectrum was recorded with low input laser fluence (~0.1 μJ/pulse) using the active attenuation technique (see the text for detail).

TABLE 1: TD/BP86 Vertical Excitation Energies and Oscillator Strengths, *f*, of the Low-Lying Excited Electronic States of BPEB, Computed at the Optimized S_0-State Geometry of D_{2h} Symmetry

state	configuration(s)	energy (eV)[a]	*f*
S_1 (B_{1u}, A′)	H → L	3.2619	1.5935
S_2 (A_g, A′)	H−1 → L, H → L+1	3.6064	0.0000
S_3 (B_{2u}, A′)	H−2 → L, H → L+4	4.0335	0.0001
S_4 (B_{3g}, A′)	H−3 → L, H → L+3	4.0346	0.0000
S_5 (B_{2u}, A′)	H → L+2	4.0434	0.0007
S_6 (B_{1g}, A″)	H−5 → L	4.1783	0.0000
S_7 (B_{3g}, A′)	H−3 → L, H → L+3	4.1967	0.0000
S_8 (B_{2u}, A′)	H−2 → L, H → L+4	4.1968	0.0132
S_9 (A_u, A″)	H−6 → L	4.2393	0.0000
S_{10} (A_g, A′)	H → L+1, H−1 → L	4.3889	0.0000
S_{11} (B_{1u}, A′)	H → L+5	4.5154	0.0169
S_{12} (B_{1u}, A′)	H−1 → L+1	4.5875	0.3095

[a] The vertical excitation energies are referred to the optimized S_0-state structures.

the dramatic decrease in fluorescence intensity at high excess energies is caused primarily by a large decrease in k_r. This decrease in k_r at higher energies cannot be attributed to intramolecular vibrational redistribution (IVR) within the $S_1(\pi\pi^*)$ manifold, as the $S_1 \rightarrow S_0$ radiative decay of IVR-produced, dark S_1 vibronic levels is expected to occur through a sequence transition (involving S_0 vibration of same symmetry), which has transition probability essentially identical to that for the "bright" vibronic level, produced by $S_1 \leftarrow S_0$ excitation. We may therefore conclude that the nonadiabatic coupling of the highly radiative $S_1(\pi\pi^*)$ state with a dark (nonradiative) electronic state leads to a dramatic dilution of radiative transition probability of vibrationally highly excited $\pi\pi^*$ state.[10]

2. Potential-Energy Profiles. Figure 2 presents the TD/BP86/cc-pVDZ potential-energy profiles of the low-lying excited singlet states of BPEB as a function of C_{Ph}—C≡C angle (θ). In the lowest-energy $\pi\sigma^*$ state, one of the two acetylene C≡C bonds is bent with θ of about 125°, whereas the other is linear ($\theta \cong 180°$), as illustrated in the figure. The preference for this geometry (as opposed to both acetylene bonds bending) can be traced to the fact that the diphenylacetylene moiety is a much better electron donor than the phenyl moiety in the $\pi \rightarrow \sigma^*$ intramolecular charge transfer (ICT) leading to the formation

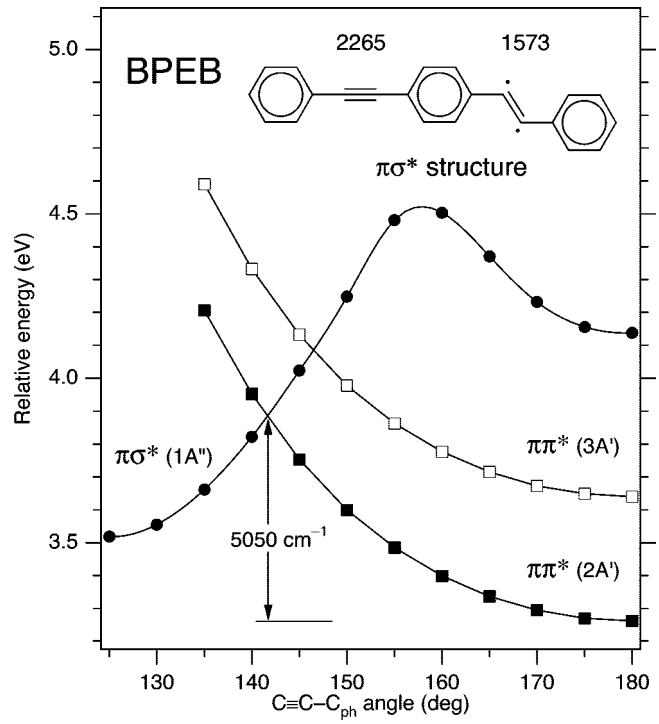

Figure 2. TD/BP86/cc-pVDZ potential-energy profiles of the low-lying electronic states of BPEB as a function of C_{Ph}—C≡C angle. The energies were calculated at the optimized ground-state geometry for a given C_{Ph}—C≡C angle. The structure in the inset is the optimized geometry of BPEB in the $\pi\sigma^*$-state minimum, with indicated CC stretch frequencies (in cm^{-1}).

of the $\pi\sigma^*$ state. As in the case of DPA, the lowest-energy $\pi\pi^*$ state crosses the $\pi\sigma^*$ state at θ between 120° and 180°. However, unlike in DPA, the lowest-energy $\pi\sigma^*$ state of bent geometry is less stable than the lowest-energy $\pi\pi^*$ state of linear geometry in BPEB. Moreover, the energy barrier for the $\pi\pi^* \rightarrow \pi\sigma^*$ state switch is significantly greater in BPEB (~0.63 eV) than in DPA (~0.29 eV), and the $\pi\pi^*/\pi\sigma^*$ intersection occurs farther away from the FC region of the initially excited $\pi\pi^*$ state ($\theta \cong 142°$ in BPEB vs $\theta \cong 155°$ in DPA). These factors are expected to render the $\pi\pi^* \rightarrow \pi\sigma^*$ state switch much less efficient in BPEB as compared to DPA. The absence of

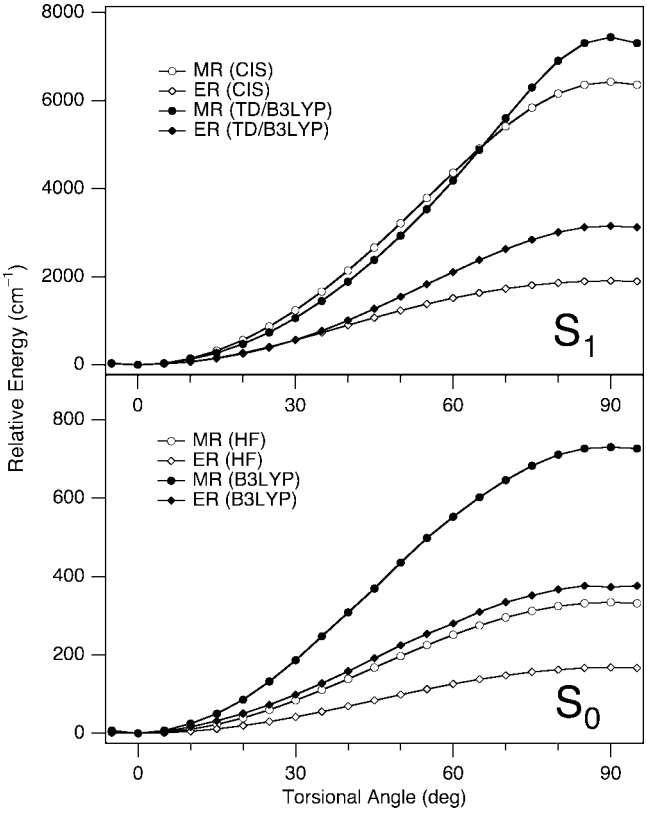

Figure 3. Torsional potentials of the S_0 and S_1 states of BPEB, as obtained from the HF/cc-pVDZ and B3LYP/cc-pVDZ, and the CIS/cc-pVDZ and TD/B3LYP/cc-pVDZ calculations, respectively. Each energy was calculated at the optimized geometry of the respective electronic (S_0 or S_1) state for a given phenyl−phenyl torsional angle. Legends: ER and MR stand for end ring and middle ring, respectively, and the notation inside the parenthesis identifies the method used for calculation.

low-energy crossing between the fluorescent $\pi\pi^*$ state and the dark $\pi\sigma^*$ state in BPEB, predicted by calculation, is consistent with the large fluorescence quantum field ($\Phi_F = 0.58$) and absence of significant thermal quenching of emission, as is the absence in picosecond transient absorption[11] of a spectral feature that can be assigned to $\pi\sigma^* \leftarrow \pi\sigma^*$ transition. Interestingly, the calculated energy barrier for the $\pi\pi^*$-state $\rightarrow$ $\pi\sigma^*$-state crossing ($\sim$5000 cm^{-1}) is in good agreement with the observed threshold energy ($\sim$4000 cm^{-1}) for the loss of fluorescence intensity and band broadening in jet-cooled BPEB.

3. Torsional Potentials of S_1 and S_0 States. The torsional motions in BPEB differ from those in DPA by the presence of the two sets of rings (end and middle). For DPA with a single set of rings, Okuyama *et al.*[6] have deduced the torsional barrier of 202 cm^{-1} for the ground state and about 1600 cm^{-1} for the $S_1(\pi\pi^*)$ state, through fluorescence jet spectroscopy. To understand the torsional motions (i.e., ring twisting) of BPEB and their effects on the spectral profiles of electronic absorption and fluorescence, we have studied the torsional potentials in both the ground and excited states within the framework of the local mode approximation. Figure 3 presents HF- and DFT-based torsional potentials for the ground-state and CIS and TDDFT torsional potentials for the lowest-energy $\pi\pi^*$ state. In both the ground and excited states, the optimized geometry was found to be planar with D_{2h} symmetry, and the low-energy torsional motion involves mostly the twisting of the end ring. Twist of the middle ring has a much greater torsional barrier. The presence of the two end-ring motions in BPEB gives rise to symmetric and antisymmetric torsional modes with differing frequencies and theoretical group representations. The asymmetric torsion involves the rotation of the end rings, whereas the symmetric torsion involves the rotation of the middle ring. This approach is different from the normal mode description of the torsional motions adapted by Greaves *et al.*,[12] which leads to vibrations that move the middle ring.

Figure 4 displays FE spectra of jet-cooled BPEB in the range of 31200−32700 cm^{-1}, measured under "cold" and "warm" beam conditions. Also shown for comparison is the cold-jet cavity ring-down (CRD) spectrum (see Supporting Information for more details) and an expanded warm-jet FE spectrum in the range of 31200−31600 cm^{-1}. It is evident that the intensity distribution of the cold-jet spectra is very similar for the FE and CRD spectra. The warm-jet FE spectrum closely mimics the CRD spectrum recently reported by Greaves *et al.*,[12] and it contains hot bands and sequence bands that are not present in the cold-jet FE and CRD spectra. Comparison of the simulated intensity distribution for the torsional progression with the warm-jet FE spectrum (or the CRD spectrum of ref 12) yields a torsional temperature of about 40 K (see Supporting Information).

Information concerning the frequencies of the ground-state asymmetric (ν_{as}) and symmetric (ν_s) torsional modes can be readily determined from the positions of the hot bands in the warm-jet FE spectrum, located at 26 and 45 cm^{-1} below the 00 $\leftarrow$ 00 ($n_s' n_{as}' \leftarrow n_s'' n_a''$) band. These bands, which can readily be identified as n_2^0 bands (00 $\leftarrow$ 20 and 00 $\leftarrow$ 02), yield $\nu_{as}'' =$ 13 cm^{-1} and $\nu_s'' = 22$ cm^{-1} if anharmonicity is neglected. These experimentally derived frequencies are in very good agreement with the HF/cc-pVDZ torsional frequencies of 13 and 19 cm^{-1}. The 13 cm^{-1} mode has nuclear displacements corresponding to the asymmetric twist, whereas the 19 cm^{-1} torsional mode moves the middle ring, consistent with the symmetric twist. The computed vibrational frequencies and their assignments are given in Table 2.

$S_1 \leftarrow S_0$ electronic transition between two torsional levels (one belonging to S_0 and the other associated with S_1) of the same symmetry is allowed by the selection rule. For BPEB with D_{2h} symmetry, the asymmetric torsional mode belongs to a_u representation, whereas the symmetric mode belongs to b_{1g} representation. As already demonstrated by Greaves *et al.*,[12] the observed torsional structures of BPEB can be assigned in terms of these torsional quantum numbers (n_s'', n_{as}'', n_s', and n_{as}'), and simulated using trigonometric potentials that describe the torsional motions. The ground-state barrier to rotations was estimated to be 220−235 cm^{-1}. The experimentally derived torsional barrier of about 230 cm^{-1} falls in between the HF derived barrier of $\sim$115 cm^{-1} and the DFT derived barrier of $\sim$375 cm^{-1} for the end ring rotation (Figure 3). In comparison, the DFT derived ground-state potential barrier for the middle ring rotation ($\sim$730 cm^{-1}) is over 3 times greater than the experiment value. For the excited state, the computed barrier heights for the end ring rotation is about 2000 cm^{-1} based on the CIS method and about 3000 cm^{-1} using the TDDFT method. The experimentally derived barrier of about 1840 cm^{-1} is very close to that based on the CIS calculation. As in the case of the ground state, the computed excited-state torsional barriers for the middle ring rotation ($\sim$6500 cm^{-1} by CIS and about 7500 cm^{-1} by TDDFT, as shown in Figure 3) are much larger than the experimentally derived barrier. Clearly, it is the end ring rotation, which is probed by experiment. The conclusion of Greaves *et al.*[12] that "the DFT derived potentials cannot be used to describe the torsional motions" is therefore invalid. The poor agreement between their calculated and experimental barriers

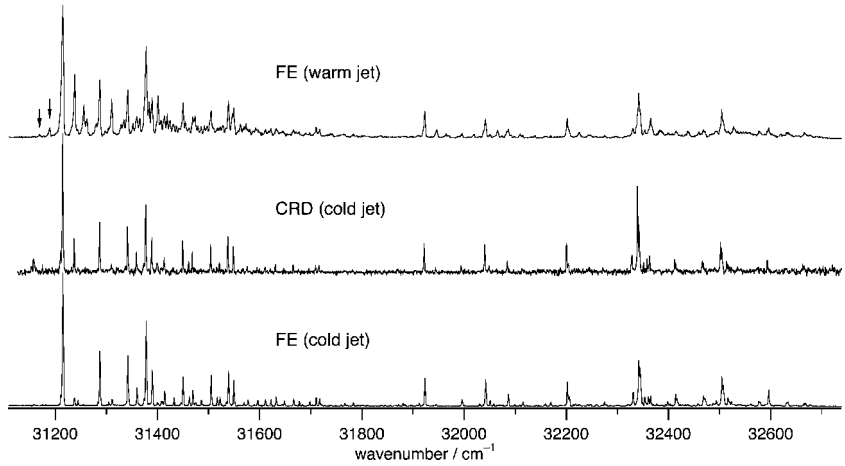

Figure 4. Comparison of the cavity ring-down (CRD) spectrum of BPEB and fluorescence excitation (FE) spectrum of jet-cooled BPEB measured under the cold-jet and warm-jet conditions. The arrows in the warm-jet FE spectrum indicate hot bands.

TABLE 2: Low Frequency (<400 cm^{-1}) HF Vibrational Modes of BPEB in the S_0 State of D_{2h} Symmetry

frequency (cm^{-1})[a]	symmetry	assignment
13	a_u	end ring asymmetric torsion
18	b_{3u}	O.P. bending of the whole molecule
19	b_{1g}	middle ring torsion
22	b_{2u}	I.P. bending of the whole molecule
50	b_{3g}	I.P. asymmetric wagging of end rings
32	b_{2g}	O.P. asymmetric wagging of end rings
104	b_{3u}	O.P. symmetric wagging of end rings
129	b_{2u}	I.P. symmetric wagging of end rings
160	a_g	harmonic stretching motion of the whole molecule
170	b_{2g}	O.P. asymmetric ethyne units bending
177	b_{3g}	I.P. ethyne units bending
263	b_{3u}	O.P. symmetric ethyne units bending
311	b_{1u}	I.P. asymmetric ethyne units stretching
340	b_{2g}	O.P. "zigzag" bending

[a] Vibrational frequencies are not scaled.

is caused not by the failure of the DFT potential, but rather by the inadequacy of the normal mode representation of the torsional motions in BPEB. Nonetheless, the DFT derived barriers for the end-ring rotations tend to be greater than the *ab initio* (HF and CIS) and the experimental barriers for both the ground and excited states of BPEB.

4. Temperature Dependence of Absorption and Fluorescence Spectra. The finding that the twisting of the end ring in BPEB is relatively free in the ground state, but strongly hindered in the excited state, has important consequences on the spectral shapes of $S_1(\pi\pi^*) \leftarrow S_0$ absorption in fluid solutions at elevated temperatures. It has been well-known from several previous studies[3,13–15] that whereas the spectral position and spectral shape of the fluorescence are insensitive to changes in temperature, those of the absorption change significantly with variations in temperatures (see Figure 5a). More specifically, the center of gravity of the absorption maximum shifts to shorter wavelengths with increasing temperature, as shown in Figure 5a. In the ground state of BPEB, the torsional barrier height ($\sim$230 cm^{-1}) is comparable to k_BT at room temperature ($\approx$200 cm^{-1}), such that the molecule exists as an equilibrium mixture of planar and various twisted conformations. The absorption spectrum of twisted molecules would be blue-shifted relative to that of planar molecule, as demonstrated by the computed torsional angle dependence of FC factor for absorption, shown in Figure 5b. The wide distribution of twisted configurations would lead to

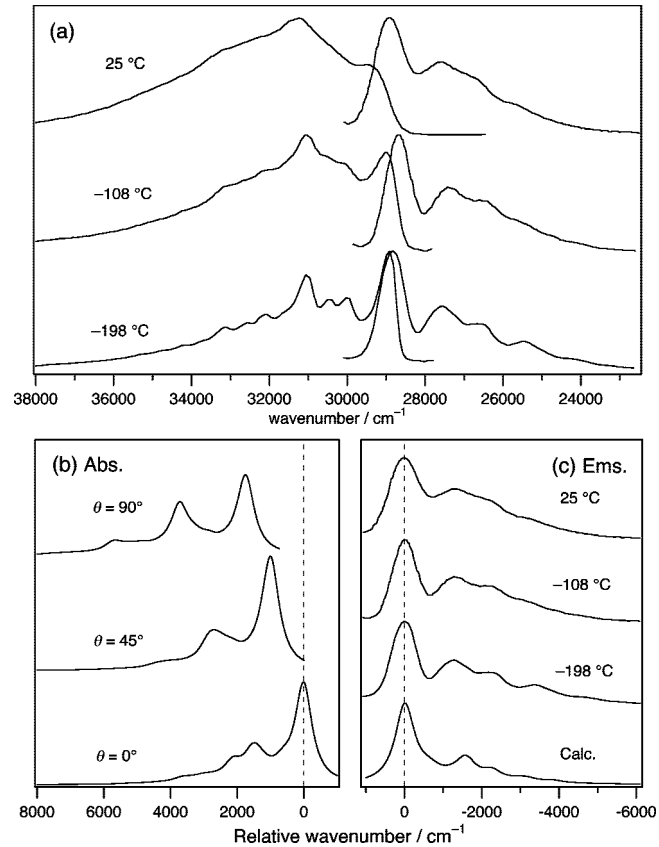

Figure 5. (a) Absorption and fluorescence spectra of BPEB in cyclohexane at three different temperatures (from ref 3 with permission). (b) Torsional angle dependence of the simulated (CIS/cc-pVDZ) absorption spectra, and (c) comparison of the vibronic structure of the simulated emission spectrum with that of the experimental spectra. The absorption and emission spectra were produced by partial optimization with a fixed angle of one end-ring to the other rings by HF/cc-pVDZ or B3LYP/cc-pVDZ for the S_0 state, and by a similar type of CIS/cc-pVDZ partial optimization for the S_1 state. The calculated vertical energies were convoluted by a Lorentzian with the line width of 300 cm^{-1}.

broadening and blue shift of the absorption spectrum with increasing temperature. The strong temperature dependence of the spectral shape of the absorption spectrum of BPEB in solution can therefore be attributed to the very shallow ground-state torsional potential (for end ring rotation) that allows significant thermal population of the higher-lying torsional levels at elevated temperatures.

Unlike the absorption spectrum, the dispersed fluorescence, originating from vibrationally relaxed excited state, is not expected to be sensitive to variation in temperature because of the steep excited-state torsional potential that favors the planar geometry. The lack of mirror symmetry relationship between the absorption and emission spectra of BPEB, in solution at elevated temperature,[3,13–15] is a consequence of the fact that although the emission originates mostly from molecules with planar conformation, the spectral profile of the absorption is strongly influenced by molecules with twisted conformations. At low temperatures where electronic absorption is dominated by low-energy planar conformer, BPEB displays the expected mirror symmetry relationship between absorption and emission,[3,13–15] as shown in Figure 5a. Figure 5c presents the computed dispersed fluorescence spectrum of the planar BPEB with the experimental spectrum, measured at low temperatures. The calculated spectra closely mimic the experimental spectrum, but the relative intensity of the 0−0 band is stronger in the computed spectrum than in the experimental spectrum. This discrepancy is most likely due to the strong overlap of the 0−0 bands of the fluorescence and absorption, which leads to a decrease in the intensity of the 0−0 band of the observed emission by self-absorption.

Conclusions

We have used the combination of quantum chemistry calculation and supersonic-jet laser spectroscopy to explore the excited-state dynamics and torsional potentials of 1,4-bis(phenylethynyl)benzene, BPEB. We found that the $\pi\pi^* \rightarrow \pi\sigma^*$ state switch, leading to fluorescence break-off, occurs at much greater $S_1(\pi\pi^*)$ excess vibrational energies in BPEB ($\sim$4000 cm^{-1}) than in diphenylacetylene ($\sim$500 cm^{-1}). The high-energy barrier for the state crossing in BEPB accounts for the large fluorescence quantum yield of BPEB ($\Phi_F = 0.58$), and the absence of $\pi\sigma^* \leftarrow \pi\sigma^*$ transition in the transient absorption spectra, measured at ambient temperature.

We studied the torsional potentials of BPEB within the framework of local mode description of the torsional vibrations. The comparison between the experimental and computed (HF and DFT for S_0 and CIS and TDDFT for S_1) torsional barriers shows overall good agreement and demonstrates that the low-energy torsional motion of the molecule involves the twisting of the end rings. The torsional barrier was found to be almost 1 order of magnitude greater in the $\pi\pi^*$ state ($\sim$2000 cm^{-1}) than in the ground state ($\sim$230 cm^{-1}). The HF/cc-pVDZ torsional frequencies (13 and 19 cm^{-1}) of the S_0 BPEB are in good agreement with the experimental frequencies (13 and 22 cm^{-1}).

The finding that the twisting of the end ring in BPEB is relatively free in the ground state, but strongly hindered in the excited state, provides a rationale for the temperature dependence of the spectral shape of absorption, and the lack of mirror symmetry relationship between the absorption and fluorescence spectra in solution at elevated temperatures.

Acknowledgment. We are grateful to the U.S. Department of Energy for support of this work, and to the Ohio Supercomputer Center for grants of computer time.

Supporting Information Available: Description of experimental setup for cavity ring-down absorption. Figures of dye laser tuning curves and their input powers, S_1 and S_0 torsional potentials and energy levels, torsional spectra at different temperatures, and potential energy profiles. Table of fluorescence lifetimes. This material is available free of charge *via* the Internet at http://pubs.acs.org.

References and Notes

(1) Schwab, P. F. H.; Levin, M. D.; Michl, J. *Chem. Rev* **1999**, *99*, 1863.
(2) Bunz, U. H. F. *Chem. Rev.* **2000**, *100*, 1605.
(3) Chu, Q.; Pang, Y. *Spectrochim. Acta, Part A* **2004**, *60*, 1459.
(4) Ferrante, C.; Kensy, U.; Dick, B. *J. Phys. Chem.* **1993**, *97*, 13457.
(5) Zgierski, M. Z.; Lim, E. C. *Chem. Phys. Lett.* **2004**, *387*, 352.
(6) Okuyama, K.; Hasegawa, T.; Ito, M.; Mikami, N. *J. Phys. Chem.* **1984**, *88*, 1711.
(7) Hirata, Y.; Okada, T.; Mataga, N.; Nomoto, T. *J. Phys. Chem.* **1992**, *96*, 6559.
(8) Hirata, Y. *Bull. Chem. Soc. Jpn.* **1999**, *72*, 1647. and references therein.
(9) Ishibashi, T.; Hamaguchi, H. *Chem. Phys. Lett.* **1997**, *264*, 551.
(10) Campos Ramos, R.; Fujiwara, T.; Zgierski, M. Z.; Lim, E. C. *J. Phys. Chem. A* **2005**, *109*, 7121.
(11) Beeby, A.; Findlay, K. S.; Low, P. J.; Marder, T. B.; Matousek, P.; Parker, A. W.; Rutter, S. R.; Towrie, M. *Chem. Commun.* **2003**, *19*, 2406. (see electronic supplementary information (ESI))
(12) Greaves, S. J.; Flynn, E. L.; Futcher, E. L.; Wrede, E.; Lydon, D. P.; Low, P. J.; Rutter, S. R.; Beeby, A. *J. Phys. Chem. A* **2006**, *110*, 2114.
(13) Beeby, A.; Findlay, K.; Low, P. J.; Marder, T. B. *J. Am. Chem. Soc.* **2002**, *124*, 8280.
(14) Levitus, M.; Schmieder, K.; Ricks, H.; Shimizu, K. D.; Bunz, U. H. F.; Garcia-Garibay, M. A. *J. Am. Chem. Soc.* **2001**, *123*, 4259.
(15) Levitus, M.; Schmieder, K.; Ricks, H.; Shimizu, K. D.; Bunz, U. H. F.; Garcia-Garibay, M. A. *J. Am. Chem. Soc.* **2002**, *124*, 8181.

JP711064G